Analyst

ROYAL SOCIETY OF CHEMISTRY

PAPER

View Article Online
View Journal | View Issue

Cite this: *Analyst*, 2023, **148**, 262

Confined surface-enhanced indole cation-radical cyclization studied by mass spectrometry†

Jianghui Sun, Hongwei Tan, Yixuan Gao, Jingjing Li, Juanjuan Wei, Shengxi Zhang, Jin Ouyang and Na Na *

Reactions in confined spaces exhibit unique reactivity, while how the confinement effect enhances reactions remains unclear. Herein, the reaction in the confined space of a nanopipette reactor was examined by *in situ* nano-electrospray mass spectrometry (nanoESI-MS). The indole cation-radical cyclization was selected as the model reaction, catalyzed by a common visible-light-harvesting complex $Ru(bpz)_3(PF_6)_2$ (1% eq.) rather than traditional harsh reaction conditions (high temperature or pressure, *etc.*). As demonstrated by *in situ* nanoESI-MS, this reaction was readily promoted in the nanopipette under mild conditions, while it was inefficient in both normal flasks and microdroplets. Both experimental and theoretical evidence demonstrated the formation of concentrated Ru(II)-complexes on the inner surface of the nanopipette, which facilitated the accelerated reactions. As a result, dissociative reactive cation radicals with lower HOMO–LUMO gap were generated from the Ru(II)-complexes by ligand-to-metal charge transfer (LMCT). Furthermore, the crucial cation radical intermediates were captured and dynamically monitored *via in situ* nanoESI-MS, responsible for the electronically matched [4 + 2] cycloaddition and subsequent intramolecular dehydrogenation. This work inspires a deeper understanding of the unique reactions in confined spaces.

Received 20th October 2022,
Accepted 26th November 2022

DOI: 10.1039/d2an01719a

rsc.li/analyst

Introduction

Confined spaces afford the focusing of various energies to command single entities, which triggers unique physicochemical properties. In tiny domains of micro/meso-porous crystalline materials,[1,2] microdroplets,[3,4] nanochannels[5–7] or nanopipettes,[8,9] single entities can be accommodated for enhanced catalytic performance, electrochemical field, optical density, and mass spectrometric signals. Specifically, compared to the bulk, catalytic reactions in confined spaces exhibit unique reactivity and selectivity under the accommodation. Therefore, confined spaces have attracted much attention to enable facile reactions, including protein degradation,[10] nanostructure formation,[11] and organic synthesis. However, the application of confined space is still in the exploratory stage due to the restricted mechanism examinations by the following factors: (1) the solution volume of reactions in tiny confined spaces is usually small, which is hard to be characterized by general methods. (2) The *in situ* capture, transmission, and interpretation of important species (including reactive radicals, intermediates, and transient catalyst complexes) are challenging during the rapid processes. (3) Dynamic reaction monitoring and mechanism examinations in confined spaces are hindered by the conflict between the ultrasmall volume of samples and the requirement of continuous injections.

Nanopipette, a controllable sharp tip with a nanometer-sized confined space, has exhibited much stronger capability for sensing, imaging, and synthesis.[12–14] As a kind of ambient mass spectrometry (AMS), nanoESI-MS was constructed by nanopipette, which has contributed to fast detection[15] and substrate screening.[8] Therefore, for reaction examinations in confined space, magic nanopipettes would exhibit at least two important roles: (1) allow *in situ* activation of substrates for reactions in confined spaces; (2) allow fast evaluation of reactions by MS detection not only in microdroplets produced by electrospray but also in confined spaces. However, most studies were concentrated on reaction acceleration in the sprayed microdroplets, while examinations of reactions in confined spaces are normally ignored. In addition, due to the difference in interface properties between microdroplets (gas–liquid) and confined nanopipette (solid–liquid), their reaction behavior would be different. Therefore, further efforts on *in situ* examination and dynamic monitoring of reactions in confined spaces are encouraged.

Herein, a generally inefficient indole cation-radical cyclization reaction was selected as a model for mechanistic studies

Key Laboratory of Radiopharmaceuticals, Ministry of Education, College of Chemistry, Beijing Normal University, Beijing 100875, China.
E-mail: nana@bnu.edu.cn

† Electronic supplementary information (ESI) available. See DOI: https://doi.org/10.1039/d2an01719a

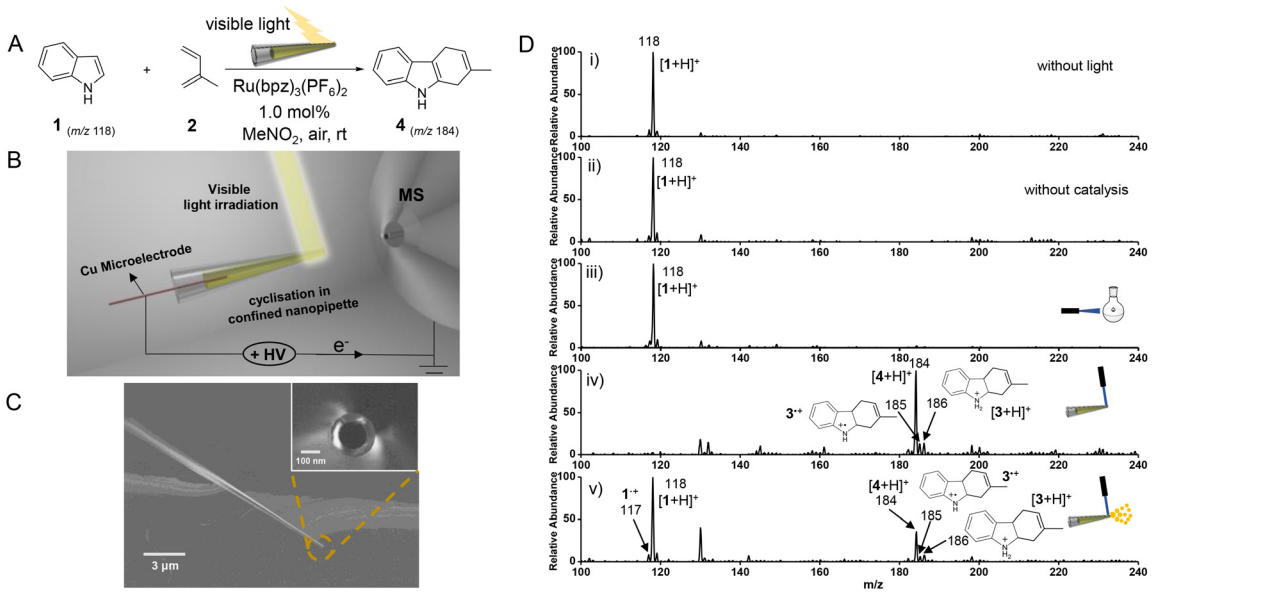

Fig. 1 (A) Scheme of the indole cation-radical cyclization catalyzed by $Ru(bpz)_3(PF_6)_2$ (1% eq.) under mild conditions. (B) Schematic diagram of nanopipette-based photocatalytic reactor and *in situ* monitoring system associated with *in situ* nanoESI-MS. (C) SEM images of nanopipette and the orifice (the inset). (D) Mass spectrometric analysis of Ru-catalyzed indole cation-radical cyclization under different conditions. Indole cation-radical cyclization in nanopipette without light irradiation (i) or without catalyst (ii), in normal flask (iii), nanopipette (iv) and microdroplets (v). All spectra were collected after reacting for 20 s.

of reactions in the confined nanopipette. Using electron-rich indole as the dienophile, this reaction was normally employed under high temperature and high pressure or modifying indole with electron-withdrawing groups.[16,17] Although ruthenium(II) polypyridyl complexes are selective catalysts, ligand modifications or hydrogen-bonding anion binders were usually required to tune electrochemical properties and ion-pairing interferences.[18,19] This makes traditional cyclization much more rigorous. In the present work, the challenging visible-light photocatalytic cyclization reaction without electro-withdrawing groups on the dienophile was commanded in a nanopipette under mild conditions (Fig. 1A). As expected, this reaction was inefficient in both normal flasks and confined microdroplets, while exhibiting enhanced reaction efficiency in the confined space. Thereby, both ambient mass spectrometric (AMS)[20,21] and theoretical examinations were employed to reveal mechanisms of enhanced reaction in the confined space.

Experimental

Regents

All reagents and solvents were purchased from commercial sources and were used without further purification unless otherwise noted. All chemicals were of analytical grade. Indole (98%, purity), $Ru(bpz)_3(PF_6)_2$, and isoprene were purchased from Sigma. Nitromethane was obtained from Innochem. Glass capillaries (i.d. 0.86 mm) were produced by Sutter Instrument (Novato, CA). Laser point (450 nm, 50 mW) was purchased from Shenzhen Infrared Laser Technology Co., Ltd, and compact fluorescent light bulb (23 W) was produced by Royal Philips. 2-Deuterated indole-d_1 (97% D) was synthesized according to the literature.[22]

Instruments and methods

All MS spectra were recorded in positive ion mode and carried out with an LTQ XL (Thermo Fisher Scientific, San Jose, CA, USA) instrument. The nanoESI emitters were constructed from glass capillaries, which were pulled to a tip using a P-1000 micropipette puller (Sutter Instrument, Novato, CA). NMR spectra were recorded on a JEOL-400 spectrometer.

Reaction preparation and procedure

In a dark hood, a solution of indole in $MeNO_2$ (0.01 M) was prepared before mixing with isoprene (5 equiv.) and $Ru(bpz)_3(BArF)_2$ (0.01 equiv.). All working solutions were prepared freshly and preserved in the dark before use. The confined-space indole cation-radical cyclization was conducted in the nanopipette, which was irradiated *via* 540 nm visible light for 20 s. Then, with the light off, 0.6 kV of the spray voltage was applied to the solution for the nanoESI-MS detection. In the microdroplet reaction, MS spectra were recorded in real time when the light and high voltage of nanoESI turned on simultaneously. Besides, the bulk reaction was conducted in a flask, which was irradiated by a compact fluorescent light bulb for 20 s. Aliquots from the flask were taken and analyzed by traditional ESI-MS in the off-line mode.

Computational procedure

All the species were optimized by employing DFT UB3LYP/Def2-SVP method. The van der Waals effects were considered

by Grimme D3 protocol. All the calculations were performed using Gaussian09 program.

Results and discussion

Construction of reaction system in confined space

As shown in Fig. 1B, a nanopipette-based photocatalytic reaction and *in situ* nanoESI-MS evaluation system were constructed. A nanopipette (140 nm, Fig. 1C) was prepared to load 1 μL dienophile indole (**1**) and diene (**2**) solution by adding $Ru(bpz)_3(PF_6)_2$ catalyst at low loadings (1% eq.). For photoexcitation, a handheld laser source, hanging vertically (~1.0 cm) on the nanopipette, offered high density and coherent visible light (450 nm, 50 mW). A Cu electrode (~0.6 kV) was inserted into the nanopipette for electrospray and subsequent MS detections. The distance between the nanotip and the MS inlet is approximately 0.7 cm. Therefore, compared to other AMSs (equipped with Venturi or ultrasonic gas-flow extraction), this system is more convenient for dynamic monitoring of short-lived intermediates in a confined space.

Reaction evaluation by *in situ* nanoESI-MS

Initially, the cyclization reactions of indole (**1**) and isoprene (**2**) were respectively employed in the flask, nanopipette, and microdroplets for comparison (Fig. 1D). The confined reaction was carried out for 20 s of light irradiation at the nanotip (Fig. 1D-iv). Thereafter, with the light off, the solution in the nanopipette was detected by *in situ* nanoESI-MS at a sample consumption rate of about 120 nL min^{-1}. As expected, the confined-space reaction did not proceed in the absence of either catalysis or visible light, where only the significant reactant ion $[\mathbf{1} + H]^+$ at *m*/*z* 118 was observed (Fig. 1D-i and ii). Similarly, after irradiating for 20 s, species in the flask were detected by traditional ESI-MS in the off-line mode. As a result, the open-chain 1,3-dienes without a rigid s-*cis*-conformation of double bonds underwent a very inefficient cyclization reaction in the normal flask (Fig. 1D-iii), consistent with the previous reports.[23] While in the presence of both catalyst and visible light irradiation in the nanopipette, the reactants were almost exhausted, and no remarkable reactant ion of $[\mathbf{1} + H]^+$ (at *m*/*z* 118) was observed after irradiating for 20 s (Fig. 1D-iv). Notably, the main ion peak was at *m*/*z* 184, and a low abundance of the desired ion at *m*/*z* 186 was observed. As deduced by collision-induced dissociation (CID) experiment, the ion at *m*/*z* 186 was attributed to the protonated [4 + 2] cycloaddition intermediate ion ($[\mathbf{3} + H]^+$) (Fig. S1-A†). The ion at *m*/*z* 184 was identified as the dehydrogenation product generated from **3** by the CID experiment (Fig. S1-B†). Furthermore, the metal electrode has little effect on the reaction, confirmed by the detection *via* inductive nanoESI, without physical contact between the electrode and solution (Fig. S2†). Therefore, in the confined space, the electron-rich indole undergoes a rapid [4 + 2] cycloaddition followed by catalytic intramolecular dehydrogenation.

Nevertheless, microdroplets from electrospray could exhibit an acceleration effect for reactions as reported previously.[15,24] To verify whether the reaction was mainly initiated by microdroplet acceleration, the reaction system was on-line detected without pre-irradiation. As shown in the inset of Fig. 1D-v, with light irradiation (on the tip) and ESI voltage simultaneously turned on, the MS spectrum was collected at 20 s. As demonstrated (Fig. 1D-v), the reaction efficiency is quite low, which exhibited the main peak of reactant indole ($[\mathbf{1} + H]^+$) at *m*/*z* 118. Furthermore, the corresponding ions of product at *m*/*z* 184 ($[\mathbf{4} + H]^+$) as well as cycloaddition intermediate ion at *m*/*z* 186 ($[\mathbf{3} + H]^+$) were quite low. As expected, when the microdroplet reaction was employed *via* shooting the light on sprayed microdroplets, no significant product ion was recorded. These could be attributed to the short reaction time during microdroplets flying from the nanotip to the MS inlet (a short distance of approximately 0.7 cm).[15] Therefore, although microdroplets were reported to exhibit high reactivities to accelerate reactions, they cannot support the satisfactory reaction efficiency for the present cyclization (Fig. 1D-iv).

Significantly, the *in situ* nanopipette-based nano-electrospray also facilitated the capture and interpretation of short-lived intermediates through MS detection. As demonstrated, other significant cationic radicals at *m*/*z* 117 (Fig. 1D-v) and *m*/*z* 185 (Fig. 1D-iv and v) were also observed. The ion at *m*/*z* 117 was ascribed to cationic radical indole$^{\bullet+}$ ($\mathbf{1}^{\bullet+}$) generated from the photo-oxidation of **1**, which evidenced the cation radical-induced cyclization. The formation of the cationic radical was confirmed by comparing the cyclization reaction with the one without light irradiation (Fig. S3†).[25,26] The ion at *m*/*z* 185 was assigned to radical $\mathbf{3}^{\bullet+}$ (Fig. S1-C†), which was afforded by the [4 + 2] cycloaddition of $\mathbf{1}^{\bullet+}$ and **2**. Further oxidation or reduction of $\mathbf{3}^{\bullet+}$ would generate the dehydrogenation product **4** or cycloaddition intermediate **3**, respectively. This indicated the generation of **4** and **3** was competitive, and the ratio of ion at *m*/*z* 184 to *m*/*z* 186 (I_{184}/I_{186}) could be used for evaluating reaction efficiencies.

Isotope labeling experiments and optimizations

To further clear the attribution of **3**, isotope labeling experiments were employed. In the experiment, 2-deuterated indole-d_1 (97% D) acted as the dienophile for the confined cyclization reaction, whose species were *in situ* monitored at interval time.[22] The structure of 2-deuterated indole-d_1 was confirmed by both NMR and ESI-MS (Fig. S4†). As shown in Fig. 2A, without light irradiation, only protonated ion of 2-deuterated indole-d_1 ($[\mathbf{1}\text{-}d_1 + H]^+$ at *m*/*z* 119 was observed (Fig. 2A-i). After 1 min of visible-light irradiation, ion at *m*/*z* 187 was observed (Fig. 2A-ii), assigned to the **3**-d_1 intermediate of isotope labeled cyclization (Fig. S1-D†). Subsequently, as the reaction continued, ions at *m*/*z* 184 and 187 increased significantly, exhibiting a comparable abundance to reactant ion (*m*/*z* 119) at 2 min (Fig. 2-iii). Significantly, after 6 min of the reaction, the product ion at *m*/*z* 184 came to be the main peak, while other ions, including reactant ion (*m*/*z* 119) and ($[\mathbf{3}\text{-}d_1 + H]^+$ (*m*/*z* 187), dramatically decreased (Fig. 2A-iv).

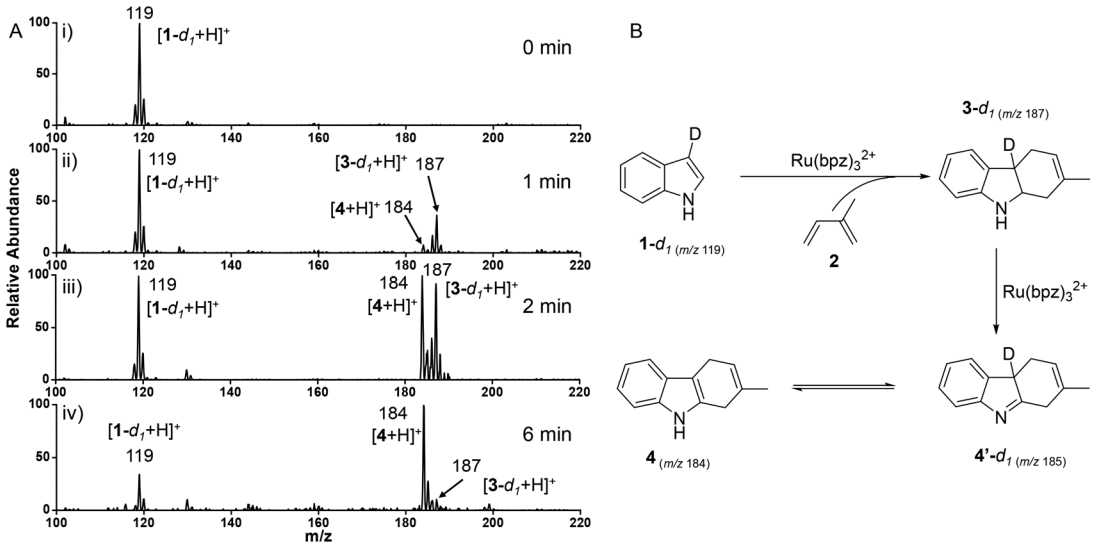

Fig. 2 Isotope labelling experiment using 2-deuterated indole-d_1 (97% D) as the dienophile. (A) The mass spectra of the reaction at different times. (B) The formation of product **4** (m/z 184) from the intermediate **3**-d_1 (m/z 187).

This result indicated the isotope labeled cyclization product of **3**-d_1 could be an intermediate to induce the formation of final product **4** (Fig. 2B). As demonstrated, **1**-d_1 (m/z 119) underwent the rapid [4 + 2] cycloaddition with isoprene (**2**), which afforded **3**-d_1 (m/z 187) generation catalyzed by Ru(bpz)$_3^{2+}$. Subsequently, two hydrogen atoms were abstracted from **3**-d_1 to form intermediate **4**-d_1′ in the presence of Ru(bpz)$_3^{2+}$. Finally, product **4** (m/z 184) could be generated by tautomerization of intermediate **4**-d_1′,[8] in accordance with the observation of the main peak at m/z 184 (Fig. 2A-iv). It should be noted that the generation of **4** without deuteration could be attributed to the rapid hydrogen–deuterium exchange or the mediation of counteranion PF_6^-.[27] The online extracted ion chromatograms (EICs) of deuterated ions also indicated the consumption of the reactant **1**-d_1 (Fig. S5-a†), along with the generation of product **4** (Fig. S5-c†). Significantly, the intensity of intermediate **3**-d_1 decreased after 1.5 min, which demonstrated its consumption for the generation of product **4** (Fig. S5-b†).

To obtain better reaction efficiency, the orifice size of the nanopipette and the volume of the reaction system were optimized. Herein, the ratios of I_{184}/I_{186} (corresponding to the ratios of final product **4** to intermediate **3**) at different conditions were calculated based on MS spectra obtained after reacting for 20 s. As shown in Fig. S6-A,† the I_{184}/I_{186} value decreased with increasing the orifice size from nanometer to micron, consistent with the enhanced reaction efficiency in confined spaces.[28–30] It should be noted that the nanoESI-MS detections were employed at high voltage from 0.6 to 0.9 kV when using nanopipettes with different orifice sizes (140 nm to 91 μm). In addition, a smaller volume of the reaction system was more convenient for obtaining higher reaction efficiency (Fig. S6-B†). This could be generated from the relatively higher light absorption efficiency and the shorter diffusion distance of the reagent in the tiny tip.[31] Therefore, 1 μL of the reaction solution was finally adopted to conduct the confined cyclization with better reaction efficiency and less operating error.

Mechanism studies of confinement effect in nanopipette

To elucidate the confinement effect of the nanopipette on the rapid cyclization reaction, ions of Ru(II)-complex were examined by *in situ* nanoESI-MS. During the reaction, the ions of m/z 288 and 576 were recorded, corresponding to Ru(II)(bpz)$_3^{2+}$ and the reduced catalyst of Ru(I)(bpz)$_3^{2+}$ (Fig. 3a). Significantly, another two complex ions at m/z 346 and 380 were well detected by the *in situ* nano-electrospray MS. Confirmed by CID experiments (Fig. S7 and S8†), the two complex ions were generated from the incorporation of Ru(bpz)$_3^{2+}$ with reactant **1** and intermediate **3**.

Subsequently, the formation of the above Ru-complexes on the inner surface of the nanopipette was studied. In fact, the nanopipette glass is not inert and could take roles during reactions,[32,33] such as the electrostatic interactions from surface silanol groups.[34] Therefore, the inner surface of the nanopipette was silanized by dichlorodimethylsilane,[35] which would avoid the electrostatic interactions from the ionization of silanol groups. Afterwards, the ions of Ru(II)-complex in the bulk reaction system, normal nanopipette, and silanized nanopipette were respectively captured for comparison. As demonstrated in Fig. 3b and c, the significant Ru(II)-complex ions of $[Ru(bpz)_3 + \mathbf{1}]^{2+}$ (m/z 346) and $[Ru(bpz)_3 + \mathbf{3}]^{2+}$ (m/z 380) were observed in the normal nanopipette. While in the normal flask and silanized nanopipette, no significant complex ion was recorded. Besides, using the silanized nanopipette, only the reactant ion of $[\mathbf{1} + H]^+$ was observed after the irradiation (Fig. S9†). Therefore, it can be concluded that the inner surface silanol of the nanopipette facilitated the formation of initial Ru-complexes with reactant and intermediate.

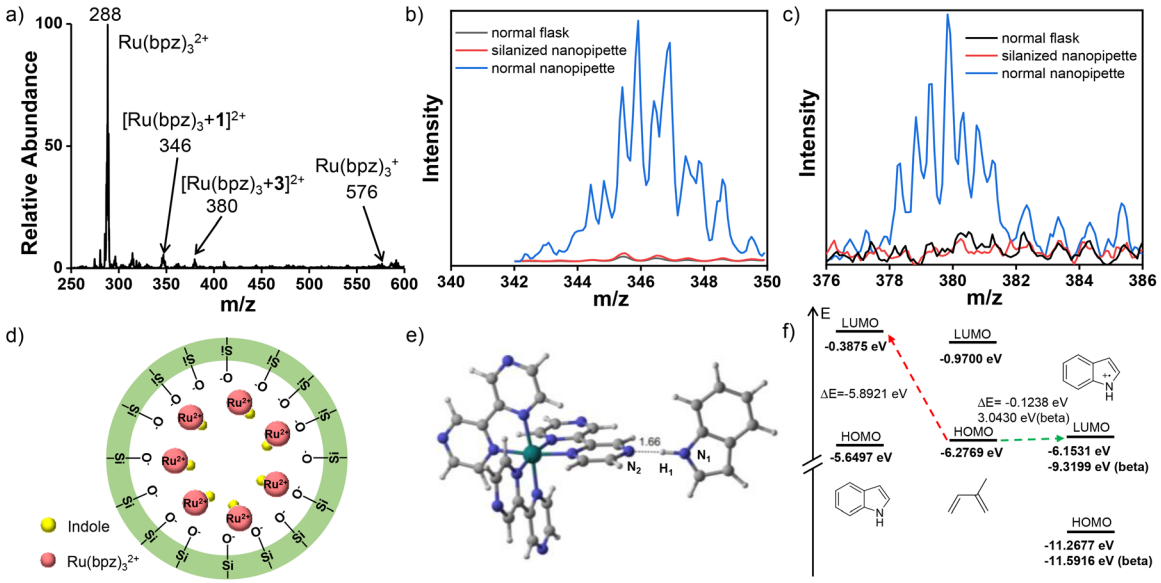

Fig. 3 Mechanism studies of confinement effect in confined space. (a) Mass spectrum of Ru(II)-complexes. (b) Ion signal of complex $[Ru(bpz)_3 + \mathbf{1}]^{2+}$ in bulk, and nanopipette with and without surface Si–OH. (c) Ion signal of $[Ru(bpz)_3 + \mathbf{3}]^{2+}$ in bulk, and nanopipette with and without surface Si–OH. (d) Illustration of the concentration of $Ru(bpz)_3^{2+}$ by surface Si–OH. (e) Calculated structure of complex $[Ru(bpz)_3 + \mathbf{1}]^{2+}$. (f) Frontier molecular orbitals of indole, indole$^{\bullet+}$ and isoprene.

Actually, the inner glass surface of the nanopipette could be negatively charged due to the ionization of silanol groups (Fig. 3d), which was also mentioned in microchannels.[36] Thereafter, the positively charged $Ru(bpz)_3^{2+}$ diffusion layer is automatically formed to give an electric double layer under the electrostatic interactions. This undoubtedly resulted in the concentrated $Ru(bpz)_3^{2+}$ catalyst on the inner surface of the nanopipette. Therefore, the locally increased catalyst concentration dramatically promoted the formation of Ru-complexes for facile oxidations, which were further examined by theoretical calculations. In addition, the present photocatalytic reaction was initiated by activating the $Ru(bpz)_3^{2+}$ catalyst *via* light absorption (Fig. 1D-i and ii), in accordance with the reports.[19] Therefore, *via* concentrating on inner surface of the nanopipette, the $Ru(bpz)_3^{2+}$ with the maximum light absorption efficiency is more likely to be greatly activated.

As demonstrated, $[Ru(bpz)_3 + \mathbf{1}]^{2+}$ was delicately obtained by covalent bonding between indole and $Ru(bpz)_3^{2+}$ *via* hydrogen bond between H1 and N2 (Fig. 3e). This was also confirmed by the CID experiment (Fig. S7†). Interestingly, calculations indicated that one β electron is transferred from **1** to $Ru(bpz)_3^{2+}$, which resulted in an approximate +1 of the spin population summed on **1**. This result indicated that dissociative radical cations of $\mathbf{1}^{\bullet+}$ could be generated from the photo-excited conversion of the complex to LMCT states.[37] This is crucial for the cation-radical initiated cyclization. The formation of radical cations $\mathbf{1}^{\bullet+}$ was further supported by studying the kinetic properties of substrates and catalyst under the theoretical level of UB3LYP/Def2-SVP.[38] Firstly, the electronic states of indole and $Ru(bpz)_3^{2+}$ were calculated to evaluate electron transformation among different valence states. As calculated, −0.377 Ha energy was released from the reduction of Ru $4d^6$ (Ru^{2+}) that was triggered by one electron transformation. This is much higher than the required energy of indole (0.279 Ha) oxidation (Table S1†), which indicates the ready generation of radical ions of $\mathbf{1}^{\bullet+}$ (*m*/*z* 117). In fact, the formation of $\mathbf{1}^{\bullet+}$ is crucial for the cyclization reaction under mild conditions.[38] As verified (Fig. 3f), the calculated HOMO–LUMO gap between diene and $\mathbf{1}^{\bullet+}$ is much lower than that between diene and indole, exhibiting electronically matched states under mild conditions. Similarly, intermediate **3** is also covalently bonded to $Ru(bpz)_3^{2+}$ *via* hydrogen bond (Fig. S10†). This promoted the formation of radical cations $\mathbf{3}^{\bullet+}$ (*m*/*z* 185) *via* LMCT (Table S1†), which facilitated the intramolecular dehydrogenation to generate final product **4**.

On-line monitoring of important reaction species in nanopipette

To further examine dynamic changes of the indole cation-radical cyclization in confined space, time-dependent profiles were obtained *via in situ* nanoESI-MS. Fig. 4 exhibits the online extracted ion chromatograms (EICs) of the reactant ion at *m*/*z* 118, the product ion at *m*/*z* 184, as well as intermediate ions at *m*/*z* 117, *m*/*z* 185 and *m*/*z* 186. As expected, upon visible light irradiation, the intensity of the reactant ion decreased gradually (Fig. 4a), accompanied by the momentary increase of cationic radical indole$^{\bullet+}$ ($\mathbf{1}^{\bullet+}$ at *m*/*z* 117) before 1 min (Fig. 4b). Along with the consumption of $\mathbf{1}^{\bullet+}$, cationic radical of ($\mathbf{3}^{\bullet+}$) at *m*/*z* 185 increased gradually within 1 min (Fig. 4c). In addition, the intermediate ion of $[\mathbf{3} + H]^+$ at *m*/*z* 186 increased after approximately 1 min (Fig. 4d), accompanied by the simultaneous decrease of $\mathbf{3}^{\bullet+}$ (Fig. 4c). Subsequently, intermediate **3**

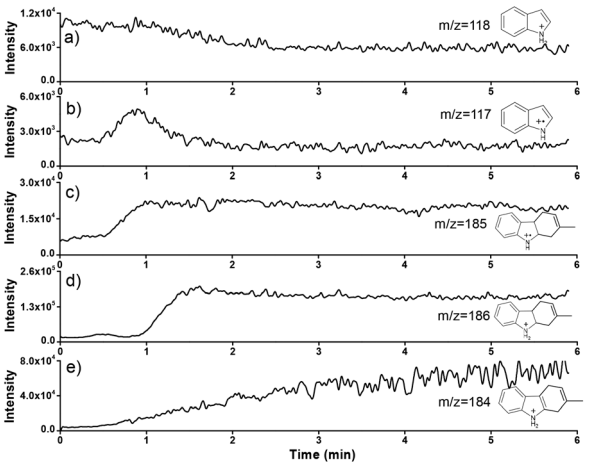

Fig. 4 Dynamic studies of different ions in confined spaces. EICs of $[\mathbf{1} + H]^+$ at *m*/*z* 118 (a), $\mathbf{1}^{\bullet+}$ at *m*/*z* 117 (b), $\mathbf{3}^{\bullet+}$ at *m*/*z* 185 (c), $[\mathbf{3} + H]^+$ at *m*/*z* 186 (d), and $[\mathbf{4} + H]^+$ at *m*/*z* 184 (e).

was consumed, and the intensity decreased gradually after approximately 1.5 min (Fig. 4d). This result also strongly verified that **3** is a relatively stable intermediate for the generation of product **4**. Undoubtedly, the product signal of $[\mathbf{4} + H]^+$ at *m*/*z* 184 kept increasing and reached the highest intensity at approximately 6 min (Fig. 4e). This time dependence property was different from the reported accelerated reactions in microdroplets within milliseconds.[10] This further excluded the possiblity of employing the present indole cation-radical cyclization in microdroplets. Therefore, the dynamic changes of different species were succesfully monitored to propose the mechanism.

Mechanism of confined cyclization reaction in nanopipette

Consequently, based on the experimental and theoretical studies, the mechanism of confined photocatalytic indole cation-radical cyclization was proposed. In the confined space (Fig. 5), the negatively charged Si–O^- layer was formed on the inner surface of the nanopipette by the ionization of silanol groups. This induced a diffusion layer of concentrated positively charged $Ru(bpz)_3^{2+}$ to form an electric double layer. The confined space of the nanopipette significantly limited the mass transfer of indole (**1**),[1] which was favorable for the formation of complex $[Ru(bpz)_3 + \mathbf{1}]^{2+}$ (*m*/*z* 346). Under photoexcitation, LMCT was initiated to form dissociative $Ru(bpz)_3^{+}$ (*m*/*z* 576) and a cationic radical $\mathbf{1}^{\bullet+}$ (*m*/*z* 117) with lower HOMO–LUMO gap for subsequent reactions.[37] Simultaneously, oxygen acts as the charge carrier to trigger the charge transfer for converting $Ru(bpz)_3^{+}$ to $Ru(bpz)_3^{2+}$.[19,38] Thereafter, in the presence of isoprene (**2**), radical $\mathbf{1}^{\bullet+}$ can rapidly undergo an electronically matched Diels–Alder reaction to generate the cationic radical $\mathbf{3}^{\bullet+}$ (*m*/*z* 185). The generated $\mathbf{3}^{\bullet+}$ could abstract one electron from another equivalent of **1** *via* the chain-propagation step (the dashed line in Fig. 5) to form $\mathbf{1}^{\bullet+}$ (*m*/*z* 117) and **3** (*m*/*z* 186).[19,26] Besides, intermediate **3** (*m*/*z* 186) could also be obtained by the reduction of $\mathbf{3}^{\bullet+}$ *via* $O_2^{\bullet-}$.[39] Similarly, the confined space also promotes the formation of complex $[Ru(bpz)_3 + \mathbf{3}]^{2+}$ (*m*/*z* 380), followed by the photoinduced LMCT to afford dissociative $\mathbf{3}^{\bullet+}$. Furthermore, $O_2^{\bullet-}$ is active in abstracting two hydrogen atoms from $\mathbf{3}^{\bullet+}$ to generate intermediate **4′** and H_2O_2. Finally, product **4** (*m*/*z* 184) was obtained *via* the tautomerization of intermediate **4′**.[8,40]

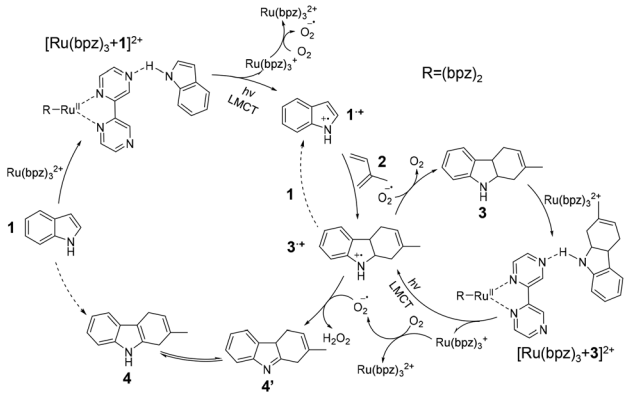

Fig. 5 Possible mechanism of the photocatalytic indole cation-radical cyclization reaction in confined space. **1–4**: reactant, intermediates and product detected by *in situ* nano-electrospray MS.

Conclusions

In summary, the enhanced indole cation-radical cyclization in the confined nanopipette was demonstrated and examined by mass spectrometry detections. As examined by the *in situ* monitoring with nanoESI-MS, new insights on the mechanism, including [4 + 2] cycloaddition and intramolecular dehydrogenation, were demonstrated. Both experimental and theoretical examinations demonstrated that an electric double layer on the inner surface of the nanopipette induces the concentration of catalysts to promote the reaction. This work has broken through the limitations on *in situ* capture, interpreting and dynamic monitoring of reactive intermediates in tiny geometric spaces. As an innovative effort to apply AMS to *in situ* examinations of the confined space, this work would inspire a deeper understanding of confinement effects.

Conflicts of interest

There are no conflicts to declare.

Acknowledgements

The authors gratefully acknowledge the financial support provided by the National Key Research and Development Program of China (No. 2019YFC1805600) and the National Natural Science Foundation of China (22274012, 21874012, 21974010).

References

1 J. Dai and H. Zhang, *Small*, 2021, **17**, 2005334.
2 T. Dwars, E. Paetzold and G. Oehme, *Angew. Chem., Int. Ed.*, 2005, **44**, 7174–7199.
3 D. B. Eremin and V. V. Fokin, *J. Am. Chem. Soc.*, 2021, **143**, 18374–18379.
4 X. Yan, R. M. Bain and R. G. Cooks, *Angew. Chem., Int. Ed.*, 2016, **55**, 12960–12972.
5 X. Wang, L. Liu, Q. Pu, Z. Zhu, G. Guo, H. Zhong and S. Liu, *J. Am. Chem. Soc.*, 2012, **134**, 7400–7405.
6 K. Qiu, T. P. Fato, B. Yuan and Y.-T. Long, *Small*, 2019, **15**, 1805426.
7 H. Song, D. L. Chen and R. F. Ismagilov, *Angew. Chem., Int. Ed.*, 2006, **45**, 7336–7356.
8 S. Chen, Q. Wan and A. K. Badu-Tawiah, *Angew. Chem., Int. Ed.*, 2016, **55**, 9345–9349.
9 E. T. Jansson, Y.-H. Lai, J. G. Santiago and R. N. Zare, *J. Am. Chem. Soc.*, 2017, **139**, 6851–6854.
10 X. Zhong, H. Chen and R. N. Zare, *Nat. Commun.*, 2020, **11**, 1049.
11 J. K. Lee, D. Samanta, H. G. Nam and R. N. Zare, *Nat. Commun.*, 2018, **9**, 1562.
12 Y. Zhang, Y. Tang, C. Tan and W. Xu, *ACS Cent. Sci.*, 2020, **6**, 1001–1008.
13 R.-J. Yu, Y.-L. Ying, R. Gao and Y.-T. Long, *Angew. Chem., Int. Ed.*, 2019, **58**, 3706–3714.
14 S.-M. Lu, Y.-Y. Peng, Y.-L. Ying and Y.-T. Long, *Anal. Chem.*, 2020, **92**, 5621–5644.
15 R. M. Bain, S. T. Ayrton and R. G. Cooks, *J. Am. Soc. Mass Spectrom.*, 2017, **28**, 1359–1364.
16 E. Wenkert, P. D. R. Moeller and S. R. Piettre, *J. Am. Chem. Soc.*, 1988, **110**, 7188–7194.
17 A. Chretien, I. Chataigner, N. L'Helias and S. R. Piettre, *J. Org. Chem.*, 2003, **68**, 7990–8002.
18 E. P. Farney, S. J. Chapman, W. B. Swords, M. D. Torelli, R. J. Hamers and T. P. Yoon, *J. Am. Chem. Soc.*, 2019, **141**, 6385–6391.
19 S. Lin, M. A. Ischay, C. G. Fry and T. P. Yoon, *J. Am. Chem. Soc.*, 2011, **133**, 19350–19353.
20 J. Sun, Y. Yin, W. Li, O. Jin and N. Na, *Mass Spectrom. Rev.*, 2022, **41**, 70–99.
21 Y. Wang, M. Sun, J. Qiao, J. Ouyang and N. Na, *Chem. Sci.*, 2018, **9**, 594–599.
22 S. A. de Keczer, T. S. Lane and M. R. Masjedizadeh, *J. Labelled Compd. Radiopharm.*, 2004, **47**, 733–740.
23 T. Peglow, S. Blechert and E. Steckhan, *Chem. Commun.*, 1999, 433–434, DOI: **10.1039/a900078j**.
24 N. Sahota, D. I. AbuSalim, M. L. Wang, C. J. Brown, Z. Zhang, T. J. El-Baba, S. P. Cook and D. E. Clemmer, *Chem. Sci.*, 2019, **10**, 4822–4827.
25 J. Sun, X. Fan, H. Lu, H. Tan, Y. Zhang, Y. Wang, Y. Zhao, J. Ouyang and N. Na, *Chem. Commun.*, 2021, **57**, 3921–3924.
26 Y. Cai, J. Wang, Y. Zhang, Z. Li, D. Hu, N. Zheng and H. Chen, *J. Am. Chem. Soc.*, 2017, **139**, 12259–12266.
27 M. Talavera, J. Bravo, L. Gonsalvi, M. Peruzzini, C. Zuccaccia and S. Bolano, *Eur. J. Inorg. Chem.*, 2014, 6268–6274, DOI: **10.1002/ejic.201402882**.
28 J. Xiao, X. Pan, S. Guo, P. Ren and X. Bao, *J. Am. Chem. Soc.*, 2015, **137**, 477–482.
29 X. Pan and X. Bao, *Chem. Commun.*, 2008, 6271–6281, DOI: **10.1039/b810994j**.
30 S. A. Miners, G. A. Rance and A. N. Khlobystov, *Chem. Sci.*, 2016, **45**, 4727–4746.
31 Q. Wan, S. Chen and A. K. Badu-Tawiah, *Chem. Sci.*, 2018, **9**, 5724–5729.
32 Y. Li, T. Mehari, Z. Wei, Y. Liu and R. G. Cooks, *Angew. Chem., Int. Ed.*, 2021, **60**, 2929–2933.
33 Y. Li, K.-H. Huang, N. M. Morato and R. G. Cooks, *Chem. Sci.*, 2021, **12**, 9816–9822.
34 N. O. Pretorius, C. M. Willemse, A. de Villiers and H. Pasch, *J. Chromatogr., A*, 2014, **1330**, 74–81.
35 B. Seed, *Current protocols in cell biology*, 2001, **Appendix 3**, 3E-Appendix 3E.
36 A. Datta, S. Gangopadhyay, H. Temkin, Q. S. Pu and S. R. Liu, *Talanta*, 2006, **68**, 659–665.
37 Q. Y. Li, S. N. Gockel, G. A. Lutovsky, K. S. DeGlopper, N. J. Baldwin, M. W. Bundesmann, J. W. Tucker, S. W. Bagley and T. P. Yoon, *Nat. Chem.*, 2022, **14**, 94–100.
38 Q. Liu, L.-J. Cheng and K. Wang, *RSC Adv.*, 2017, **7**, 30618–30625.
39 Y. Zhao and M. Antonietti, *Angew. Chem., Int. Ed.*, 2017, **56**, 9336–9340.
40 S. Jayaraj and A. K. Badu-Tawiah, *Sci. Rep.*, 2019, **9**, 11280.